Kai Wu, Jacopo Pegoraro, Francesca Meneghello, J. Andrew Zhang, Jesus O. Lacruz, Joerg Widmer, Francesco Restuccia, Michele Rossi, Xiaojing Huang, Daqing Zhang, Giuseppe Caire, and Y. Jay Guo

Sensing in Bistatic ISAC Systems With Clock Asynchronism

A signal processing perspective

©SHUTTERSTOCK.COM/CINEMANIKOR

Integrated sensing and communication (ISAC) has been identified as a pillar usage scenario for the impending 6G era. Bistatic sensing, a major type of sensing in ISAC, is promising to expedite ISAC in the near future as it requires minimal changes to the existing network infrastructure. However, a critical challenge for bistatic sensing is clock asynchronism due to the use of different clocks at far-separated transmitters (Txs) and receivers (Rxs). This causes the received signal to be affected by time-varying random phase offsets, severely degrading—or even failing—direct sensing. Hence, to effectively enable ISAC, considerable research has been directed toward addressing the clock asynchronism issue in bistatic sensing. This article provides an overview of the issue and existing techniques developed in an ISAC background. Based on the review and comparison, we also draw insights into the future research directions and open problems, aiming to nurture the maturation of bistatic sensing in ISAC.

Introduction

Communications-centric ISAC systems are expected to deliver a ubiquitous radio sensing network without notably affecting communication performance. These systems have sparked the rise of a novel technological paradigm that seamlessly integrates wireless sensing into next-generation mobile networks. This integration holds the potential to significantly enhance a diverse range of contemporary smart applications [1], [2], [3]. A prominent example is the implementation of ISAC in mobile networks, termed the *perceptive mobile network* (*PMN*). Since its inception in 2017 [4], the PMN has captured substantial attention from academia and industry alike. An important milestone occurred in June 2023 when the International Telecommunication Union (ITU) greenlighted the 6G vision framework, where the concept of ISAC has been identified as one of the six pivotal usage scenarios for the impending 6G era, also denoted by IMT-2030 [5].

Many sensing approaches are possible in the PMN [3], including monostatic sensing at a single base station or bistatic sensing between base stations or between a mobile

Digital Object Identifier 10.1109/MSP.2024.3418725
Date of current version: 21 November 2024

device—user equipment (UE)—and a base station. Bistatic sensing configurations are particularly promising for seamlessly integrating sensing into communications. This approach boasts compelling advantages. It requires almost no change to the current network infrastructure, alleviating the formidable demands of challenging technologies such as full-duplex mobile transceivers. In particular, when the bistatic configuration includes a UE as the Tx, sensing functions benefit from the spatial, spectral, and temporal diversities in user signals, thereby embracing the potency of networked and fused sensing methodologies. Moreover, performing sensing functionalities at the base station is more feasible as these are equipped with heightened sensing capacities encompassing more advanced power, computational resources, and networking capabilities.

One critical challenge for bistatic sensing is clock asynchronism due to the bistatic ISAC setup. The bistatic Tx and sensing Rx, regardless of whether they are base stations or UEs, are spatially separated, and their clocks from the local oscillators (LOs) are not locked and asynchronous. Clock asynchronism causes timing offset (TO), carrier frequency offset (CFO), and random phase shifts across discontinuous transmissions, which hinder the coherent processing of discontinuous channel measurements and introduce ambiguities into sensing results. This is a common problem in almost all communications-centric ISAC systems. Still, it is more prominent in mobile networks due to the typically wide separation of Txs and Rxs, the mobility of nodes, and the absence of line-of-sight (LoS) connections. Should this problem be efficiently solved, sensing could be seamlessly realized in communication networks via software running in base stations with enhanced computing capabilities.

Considerable research has been directed toward bistatic sensing in ISAC systems to tackle this challenge. These efforts have led to some preliminary solutions, which were partially and conceptually reviewed in an early article [6]. However, these solutions have various limitations, and practically viable solutions are yet to be developed. In this article, we offer an all-encompassing and meticulous exploration of signal processing techniques for the compensation and removal of TO, CFO, and phase offsets in bistatic sensing. Specifically, this article encompasses ISAC signal processing architectures within contemporary and futuristic mobile networks, which may be applied to any bistatic scenario without requiring cooperation or active signaling among nodes (also called the *single-node* scenario). This article is also devoted to thoroughly covering pertinent contributions from the existing open literature, coupled with the sharing of our own reservoir of research experiences, outcomes, and forward-looking visions. Note that while most wireless sensing literature addresses the clock asynchronism challenge in Wi-Fi networks, the approaches can potentially be applied to mobile networks given their similar physical-layer techniques. More detailed comparisons between the two networks will be provided in the "Single-Node Bistatic Sensing Techniques" section. Overall, we hope that our work will contribute to the maturation of ISAC technology in the near future.

The rest of this article is organized as follows. In the "Clock Asynchronism and its Modeling in Bistatic Sensing" section, we introduce the different phase offsets caused by clock asynchronism and establish the basic reference channel frequency response (CFR) model used in this article. A detailed review of three main approaches for eliminating such phase offsets is carried out in the "Single-Node Bistatic Sensing Techniques" section, analyzing and comparing numerous works from the related literature. In the "Future Research Directions and Open Problems" section, we generalize a technical framework and outline six key challenges for future research, focusing on the limitations of the reviewed methods. Finally, we give concluding remarks in the "Concluding Remarks" section.

Clock Asynchronism and Its Modeling in Bistatic Sensing

Offsets Caused by Clock Asynchronism

The basic clock is typically generated from the LO to support various operations in a radio device. Clock asynchronism happens when the basic clocks of the Tx and Rx are not locked in phase or frequency. This introduces unwanted offsets in the received signals—including but not limited to CFO, TO, and phase offsets—as detailed next.

- *CFO:* CFO is mainly caused by the difference between the LOs of the Tx and Rx. Since no two oscillators can generate the same frequency, the carrier frequencies generated by two independent oscillators will also differ, yielding CFO. Moreover, due to environmental factors such as temperature changes, supply voltage variations, and aging, oscillator frequency can drift slowly, leading to a slow-varying CFO between a pair of Txs and Rxs. It is typically estimated using, e.g., two segments of repeated signals in communication systems. This estimation can then be used to compensate for the CFO. However, the inevitable estimation error leads to residual CFO, which may become fast time varying due to the variation of CFO estimation.
- *TO:* TO results from the lack of a synchronized time reference between the Tx and Rx as they use their own LOs to generate the necessary timing signals for transmitting and receiving signals. Due to independent clock sources, there can be an unknown shift or offset in the time perceived by the Rx compared to the actual transmission time. Such TO is almost unchanged during continuous transmission and reception; however, it may become time varying during discontinuous transmission, particularly when a node transits between transmission and reception. In addition, the change of the synchronization point used in the Rx also introduces time-varying TO. The fine-timing point may slightly vary in position due to, e.g., random noise, even if the channel is unchanged, particularly in orthogonal frequency division multiplexing (OFDM) systems with many subcarriers.
- *Phase offset:* The phase offset can be caused by transceiving electronic devices and the inherent phase noises of LOs. The factors contributing to these noises, such as thermal noise and flicker noise, are inherently rapid and stochastic, making phase offset fast varying, possibly on a symbol basis.

Considering the different contributing factors to the three offsets, we can conclude the following:

- CFO changes on a time scale of minutes to hours due to gradual factors like temperature changes and component aging, but residual CFO after compensation can change on a millisecond time scale.
- TO changes on a time scale of milliseconds to seconds as it can be influenced by slow-varying oscillator drift, transition between transmission and reception, and shift of the fine-timing point.
- Phase offset changes on a time scale of microseconds as it results from rapid and intrinsic noise fluctuations within LO and electronic circuits.

Figure 1 illustrates the phases of the channel state information (CSI) estimates over OFDM subcarriers and consecutive symbols for long-term evolution (LTE) and Wi-Fi signals in static environments. The phases contain the effects of all the offsets mentioned previously. For LTE, which has a stringent time slot structure, multiple frames (each containing 20 slots) are transmitted continuously. Each frame starts with a downlink slot, followed by uplink slots. The cell-specific reference signals are used for channel estimation, leading to 40 CSI estimation vectors per frame (two symbols with reference signals in each slot). Each vector consists of CSI estimates over subcarriers. Four subcarriers are evenly selected over all resource elements for the illustration in Figure 1(a). The figure shows that the LTE CSI phase slowly varies over time during continuous transmission, but it suffers from rapid changes corresponding to the uplink-downlink transition.

During continuous transmission, phase offset variations are slow, as can be seen from the phases of each subcarrier; TO also varies slowly, as can be seen from the slow variations of the relative phase differences between the four subcarriers. For Wi-Fi, random packet transmission is performed in the CSI extraction to emulate practical Wi-Fi scenarios. For clarity, two subcarriers (in different colors) are selected for illustration. We see that the CSI phase rapidly changes over time slots and subcarriers, both in random manners, suggesting fast time-varying phase offset and TO. The results in Figure 1 intuitively manifest the impact of the three offsets illustrated previously on bistatic sensing signals.

Signal Modeling

We now incorporate these offsets into a multiple-input, multiple-output (MIMO) OFDM ISAC signal model. We note that MIMO-OFDM has been extensively used in modern cellular networks, such as 4G and 5G. It is foreseeable to continue prevailing in 6G. Consider a two-node MIMO-OFDM communication system where the transmitting and receiving nodes are each equipped with a uniform linear array. The Tx (Rx) array has M (N) antennas with a half-wavelength antenna spacing. Their steering vector can be given by $\mathbf{a}(x, \alpha) = [1, e^{j\pi\sin(\alpha)}, \ldots, e^{j(x-1)\pi\sin(\alpha)}]^{\mathrm{T}}$, $x = M$ or N, where α can be the angle of departure (AoD) or angle of arrival (AoA). For OFDM transmissions, the frequency band with bandwidth B is divided into S subcarriers. The subcarrier interval is then $\Delta_f = B/S$, leading to an OFDM symbol period of $T_O = T_0 + T_{\mathrm{cp}}$, where $T_0 = 1/\Delta_f = S/B$, and T_{cp} is the period of the cyclic prefix.

Consider $k = 1, \ldots, K$ received OFDM symbols, equally spaced at an interval of T_s. Denote the TO and (residual) CFO as $\tau_{\mathrm{o},k}$ and $f_{\mathrm{o},k}$, respectively. Moreover, we use β_k, a complex value, to reflect random phase offset and all other hardware imperfections (to sensing), such as automatic gain control, RF chain imbalance, etc. Note that all these nuisances depend on the relative asynchrony between the Tx and the Rx; hence, they are specific to each Tx-Rx pair. Moreover, they are time varying on an OFDM symbol level, as indicated by their subscript k. Assume that there are L paths, where the lth ($l = 1, \ldots, L$) path's complex path gain, propagation delay, Doppler frequency, AoA, and AoD are given by b_l, τ_l, $f_{D,l}, \phi_l$ and θ_l, respectively. The noise-free CFR matrix at the ith subcarrier and kth OFDM symbol can be expressed as

$$\mathbf{H}_{i,k} = \beta_k \sum_{l=1}^{L} b_l e^{-j2\pi i(\tau_l+\tau_{\mathrm{o},k})\Delta_f} e^{j2\pi(f_{D,l}+f_{\mathrm{o},k})kT_s} \mathbf{a}(N, \phi_l)\mathbf{a}^{\mathrm{T}}(M, \theta_l) \tag{1}$$

$$= \underbrace{\beta_k e^{-j2\pi i\Delta_f\tau_{\mathrm{o},k}} e^{j2\pi f_{\mathrm{o},k}kT_s}}_{\xi_{i,k}} \sum_{l=1}^{L} b_l e^{-j2\pi i\Delta_f\tau_l} e^{j2\pi f_{D,l}kT_s} \mathbf{a}(N, \phi_l)\mathbf{a}^{\mathrm{T}}(M, \theta_l). \tag{2}$$

Three assumptions have been made here.

1) All transmitting antennas share a common LO, and all receiving antennas do so as well.
2) The intrasymbol phase change caused by the Doppler frequency and CFO is negligible.
3) The sensing parameters of the targets can be considered constant within a short coherent processing interval, such as over a period from several to tens of milliseconds [7].

Thus, their dependence on the symbol index k is suppressed in $\mathbf{H}_{i,k}$ for brevity. All three assumptions are typical and widely

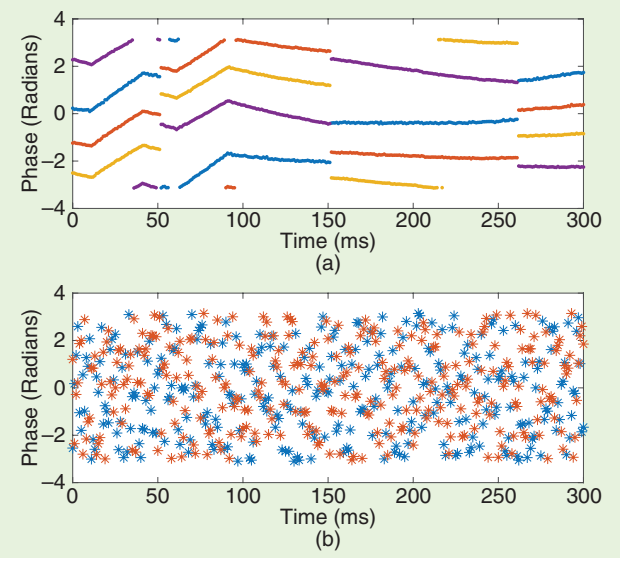

FIGURE 1. Time-varying phases of (a) LTE and (b) Wi-Fi CSIs extracted from the National Instrument MIMO testbed and a commercial Wi-Fi platform, respectively. Four different colors are for four equally spaced subcarriers. (a) Time-division duplexing LTE. (b) Wi-Fi.

used in most radar and ISAC work. In (2), several nuisance coefficients are combined into a single term, as denoted by $\xi_{i,k}$.

The L paths in (2) can be grouped into static and dynamic paths, depending on whether the underlying scatterer is moving during the observation time period or not. Note that one observation period can consist of multiple OFDM slots or packets. For static paths, we have $f_{D,l} = 0$, and τ_l, θ_l, ϕ_l remain constant over the whole observation period. For a dynamic path $f_{D,l} \neq 0$, the sensing parameters can be considered constant within a short processing interval, as done in (2). Over the observation period, the sensing parameters may change, as shown later in the "Offset Cancellation Methods: Spatial-Domain Processing" section. These properties are key to some of the methods presented in the "Single-Node Bistatic Sensing Techniques" section.

The offsets due to clock asynchronism generally degrade sensing. On the one hand, TO and CFO cause an ambiguity value in delay and Doppler frequency estimation, leading to ambiguity in ranging and speed estimation. On the other hand, the random phase offsets make it impossible to process multiple CSI measurements coherently directly; note that CSI power can be exploited for jointly processing multiple measurements in the temporal domain. Moreover, popular advanced sensing techniques from radar sensing, such as the micro-Doppler spectrogram [8], are also severely affected by CFO, which destroys Doppler features. The micro-Doppler contains fine-grained information on targets, including multiple moving parts. It is a key component of many applications, such as target recognition, human activity recognition, and person identification, among others [2]. We will use the quality of the micro-Doppler as one of the possible evaluation criteria and a means of comparison for CFO removal techniques.

Challenges in Addressing Clock Asynchronism for Sensing

In communications systems, the aforementioned offsets due to clock asynchronism are compensated for by using well-established algorithms [9], [10], [11]. Moreover, there is no need to separate TO from the propagation delay for communications. The Rx determines the fine timing, and the remaining TOs are included in the channel estimation and removed via channel equalization. For CFO, it can be estimated and compensated by using, e.g., two repeated sequences [11], and the impact of residual CFO, together with a small Doppler shift, may be ignored or mitigated via estimating and compensating their accumulated phase shift.

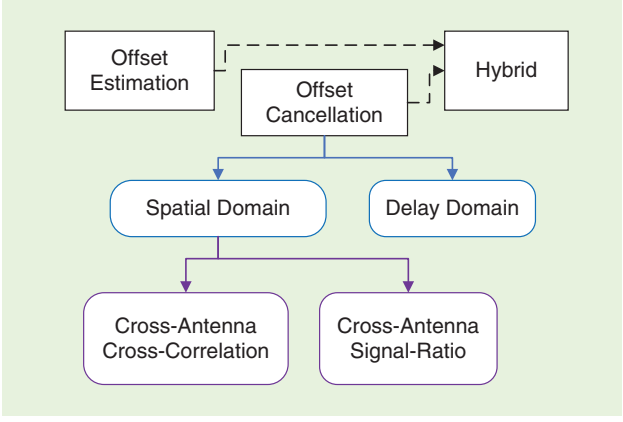

FIGURE 2. The classification of single-node bistatic sensing techniques that tackle the clock asynchronism problem.

Unlike data communications, where the offsets can be treated effectively in general, mitigating the impacts of such offsets on sensing is challenging. For sensing, the TO has to be separated to get a clean estimate for propagation delays. The CFO and f_D also need to be separated for sensing, and this cannot be achieved via the conventional CFO estimation technique. The residual CFO may have a close value to the Doppler shifts to be estimated, causing large Doppler estimation errors if not handled properly. Therefore, addressing clock asynchronism is a critical challenge in bistatic sensing.

Several approaches can potentially address this problem [6], such as using a global GPS disciplined clock (GPSDO) or applying single-node-based signal processing techniques. A GPSDO with a timing accuracy of up to 5.5 ns can cost US$1,000 [6]. It also requires an open-sky view to operate, and its size is relatively large. Therefore, it cannot be practically integrated into every mobile device. In comparison, single-node-based processing can be more practical and promising in addressing the asynchronism challenge at a much lower cost as it does not require additional devices or complex information exchange between multiple nodes. However, the GPSDO is not without merits. In scenarios such as a large shopping mall, investing in a high-quality GPSDO may enable the distribution of a precise clock to many terminals via wires, improving clock stability for better bistatic sensing. This work mainly focuses on signal processing techniques for addressing the clock asynchronism issue. Next, we provide an in-depth overview of the techniques.

Single-Node Bistatic Sensing Techniques

From the signal processing perspective, addressing the clock asynchronism issue in bistatic sensing can be achieved by eliminating the contribution of $\xi_{i,k}$ in (2). The elimination can be achieved via either cancellation without estimating the values or estimation followed by compensation; it can also be done in different domains, such as spatial and delay domains. Depending on how the "elimination" is achieved, we organize and present the techniques, as found in the literature, through three major types of methods, as summarized in Figure 2.

1) *Offset cancellation methods [12], [13], [14], [15], [16], [17], [18]:* This approach is predominantly applied in the spatial domain [12], [13], [14], [15], [16], [17], utilizing the fact that the clock asynchronism term, $\xi_{i,k}$, is common over antennas and can be mitigated through cross-antenna processing, including cross-correlation and signal ratio. Recently, an offset cancellation in the delay domain has been proposed [18] that does not require multiple receiving antennas.
2) *Offset estimation and suppression [19], [20], [21]:* These methods estimate the nuisance terms, namely $\tau_{o,k}$ and $f_{o,k}$, separately or their composite impact, $\xi_{i,k}$, as an integral and then mitigate them to facilitate unambiguous sensing.

3) *Hybrid of offset cancellation and estimation [22]:* This type of method estimates and suppresses the TO, while CFO is cancelled out similarly to point 1). Since the nuisance term, $\xi_{i,k}$, is common to all the propagation paths, delay-domain processing of the channel impulse response (CIR) is used to obtain the TO efficiently through correlation. A reference static path is then used to cancel out the phase offsets without requiring the availability of multiple antennas at the Rx.

Each technique has specific features, advantages, and disadvantages, and their applicability depends on the sensing objectives. For example, some techniques may be suitable for obtaining estimates for some specific parameters, such as AoA and delay. Still, they may not be able to enable coherent signal processing over the temporal domains. Next, we review some representative works on the three types in more detail. Note that the different approaches will be analyzed based on the strategy used to tackle the clock asynchronism and estimate the multipath propagation parameters, i.e., the paths' complex path gain, propagation delay, Doppler frequency, AoA, and AoD, as described in the CFR model in (2). The target information regarding environmental position and movements can be obtained by applying further processing steps to the estimated propagation parameters. This processing can be independent of the estimation procedure. We refer interested readers to [22] for this aspect.

Offset Cancellation Methods: Spatial-Domain Processing

Cross-Antenna Cross-Correlation

For clarity in reviewing the core idea of cross-antenna cross-correlation (CACC) [12], we simplify $\mathbf{H}_{i,k}$ in (1) by assuming a single transmitting antenna, i.e., $M = 1$. Then, the channel coefficient of the nth antenna at the ith subcarrier and kth OFDM symbol can be written into

$$H_{i,k,n} = \xi_{i,k} \sum_{l=1}^{L} b_l e^{-j2\pi i \Delta_f \tau_l} e^{j2\pi f_{D,l} k T_s} e^{jn\pi \sin(\phi_l)}. \tag{3}$$

By name, CACC takes the conjugate cross-correlation of the channel coefficients between two antennas. One antenna is considered as a reference and given index $n = 0$ by convention. Let us consider the cross-correlation between $H_{i,k,0}$, i.e., $n = 0$, with $H_{i,k,n}$, where $n \neq 0$. The CACC based on $H_{i,k,n}$ can be calculated as

$$r_{i,k,n} = H_{i,k,0} H^*_{i,k,n} \approx \sum_{l_1=1}^{L} \sum_{l_2=1}^{L} b_{l_1} b^*_{l_2} e^{-j2\pi i \Delta_f (\tau_{l_1} - \tau_{l_2})} e^{j2\pi (f_{D,l_1} - f_{D,l_2}) k T_s} e^{-jn\pi \sin(\phi_{l_2})} \tag{4}$$

where the approximation is due to $|\xi_{i,k}|^2 \approx 1$. The phase offset is fully mitigated from $r_{i,k,n}$. However, its cross-products also introduce more unknown parameters by creating virtual paths. Numerous designs have been proposed in the literature to efficiently estimate the true target parameters from $r_{i,k,n}$ [12], [13], [14].

In [12] and [13], a strong LoS is assumed to be present, a single dynamic path is considered, and the L paths in (3) are divided into two groups: static paths and a single dynamic path. Then, $r_{i,k,n}$ in (4) has four main components.

1) Static paths on antenna $n = 0$ times the conjugate of static paths on antenna n: In the presence of a strong LoS, this product is approximately constant over time and can be suppressed using a high-pass filter.
2) The dynamic path on the antenna $n = 0$ times the conjugate of the dynamic path on the antenna n: This product is much weaker than the other three involving the strong LoS-dominant static path and hence can be ignored.
3) Static paths on the antenna $n = 0$ times the conjugate of the dynamic path on the antenna n: This product includes the dynamic path's sensing parameters, which have opposite signs to actual ones due to the conjugate operation. Its power is also dominated by the static path on antenna 0.
4) The dynamic path on antenna 0 times the conjugate of static paths on antenna n: This product reflects true sensing parameters with power dominated by the static paths on antenna n.

Based on the previous four components' features, an add-minus sensing method (AMS) is proposed in [12]. As can be seen from the power features of the last two components mentioned previously, adding a positive value to antenna n can enhance the last component, and subtracting a positive value from antenna 0 can weaken the third component with the virtual target. This then facilitates the estimation of the actual target's sensing parameters based on CACC. Unlike AMS, the work in [13] proposes utilizing the other components listed previously to mitigate unwanted terms. In particular, the authors of [13] reveal that, in the presence of a strong LoS path, the second-order cyclic differences of all cross-correlations over adjacent antennas can be used for estimating the terms related to the virtual targets in the first-order difference. The estimation can then be used to mitigate the impact of virtual targets in the first-order differences, facilitating the unambiguous Doppler frequency estimation using the root-MUSIC algorithm.

Different from the aforementioned work focusing on a single dynamic path, the work in [14] constructs new signals based on CACC results in such a way that the constructed signals are spanned by the same number of bases as that of the dynamic paths. A mirrored MUSIC algorithm is then proposed to estimate the Doppler frequencies of multiple targets.

If multiple snapshots are exploited to generate AoA estimates only, we can compute the conventional spatial correlation matrix $(1/K)\sum_{k=k_0}^{k_0+K-1} \mathbf{H}_{i,k} \mathbf{H}_{i,k}^H$, where all offsets are cancelled as CACC is implicitly applied. Thus, conventional spectrum analysis techniques such as MUSIC can be applied to obtain the estimates. However, it is important to note that the cross-correlation terms from K snapshots are averaged as the output, preventing the application of a bandpass filter to eliminate static components. Fortunately, as shown in [20], all static components can be estimated as one element in the MUSIC spectrum domain as they appear as one constant vector in all snapshots.

Cross-Antenna Signal Ratio

Similar to CACC, the cross-antenna signal ratio (CASR) [15] utilizes the fact that the phase offset caused by asynchronism is common to all receiving antennas; the ratio between two antennas can cancel out the asynchronism factors, i.e., $\xi_{i,k}$ in (2), facilitating unambiguous sensing. Similar to how we obtain $r_{i,k,n}$ in (4), the ratio between $H_{i,k,n}$ and $H_{i,k,0}$ provides the following CASR formulation:

$$\rho_{i,k,n} = \frac{H_{i,k,n}}{H_{i,k,0}} = \frac{\sum_{l=1}^{L} b_l e^{-j2\pi i \Delta_f \tau_l} e^{j2\pi f_{D,l} k T_s} e^{jn\pi \sin(\phi_l)}}{\sum_{l=1}^{L} b_l e^{-j2\pi i \Delta_f \tau_l} e^{j2\pi f_{D,l} k T_s}} \tag{5}$$

where $\xi_{i,k}$ is cancelled out, but the sensing parameters appear in the denominator. The latter change makes CASR a nonlinear model of sensing parameters, invalidating numerous conventional sensing methods based on a linear sensing model.

Assuming a single dynamic path and combining all static paths into a single term, the CASR formulation mentioned previously can be simplified as

$$\rho_{i,k,n} = \frac{\tilde{b} e^{jn\pi \sin(\phi_l)} e^{j2\pi f_{D,l} k T_s} + \mathcal{A}}{\tilde{b} e^{j2\pi f_{D,l} k T_s} + \mathcal{B}} \tag{6}$$

where $\mathcal{A}$ and $\mathcal{B}$ are independent of $f_{D,l}$. It is pointed out in [15] that, if $\mathcal{A}\tilde{b}e^{j2\pi f_{D,l} k T_s} - \mathcal{B}\tilde{b}e^{jn\pi \sin(\phi_l)} \neq 0$, $\rho_{i,k,n}$ is the Mobius transformation of $e^{j2\pi f_{D,l} k T_s}$. Through analyzing the different impacts of translation, complex inversion, and multiplication operations involved in a Mobius transformation, it is revealed that the CASR and $e^{j2\pi f_{D,l} k T_s}$ span the same angular range in the complex domain. In the case of a single dynamic path, as considered in [15], the absolute CASR presents a sinusoidal-like oscillation, and the peak-to-peak magnitude of the oscillation can be enhanced by rotating the CASR in the complex domain. After searching for the optimal rotation, the autocorrelation of the absolute CASR over symbols is used to estimate the dynamic path's Doppler frequency.

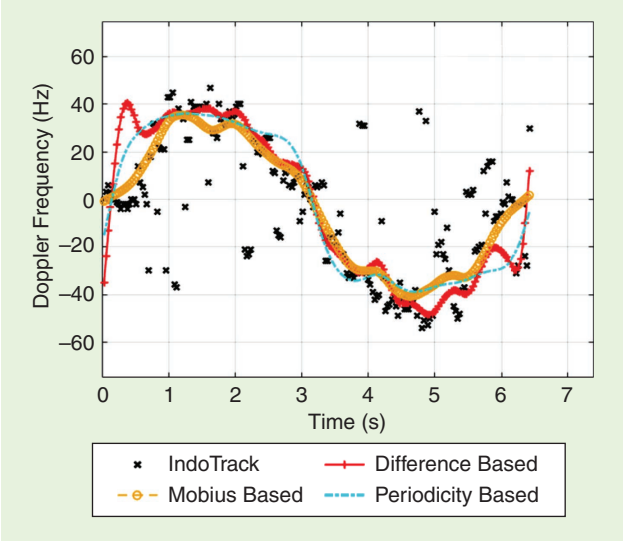

FIGURE 3. The CASR-based Doppler estimation, in comparison with CACC-based estimation in a classroom setting [16], based on the Widar dataset [23]. As shown in [21], one can use the ground truth locations, along with timestamps, published in [23] for calculating the true Doppler frequencies.

In [16], three estimation methods are proposed to estimate the Doppler frequency of a single target based on the CSI ratio. The first method estimates the angular change of $\rho_{i,k,n}$ over a time interval, say Δ_t, and then performs the linear fitting to estimate the changing rate of the phase as the Doppler frequency. Note that, to estimate the angular change over time, the center of the arc/circle generated by $\rho_{i,k,n}$ must be estimated first. The second method is built on the same periodicity between $\rho_{i,k,n}$ and $e^{j2\pi f_{D,l} k T_s}$. It proposes to estimate the periodicity of $\rho_{i,k,n}$ over k by searching for the time interval leading to the closest angles of $\rho_{i,k,n}$. The third method utilizes the periodicity of $\rho_{i,k,n}$ and searches the time interval leading to the minimum cross-correlation between $\rho_{i,k,n}$ and its delayed version.

When tested on the public Widar2.0 Wi-Fi dataset [23], the three Doppler estimation methods proposed in [16] outperform the IndoTrack based on CACC [12] in indoor scenarios, as illustrated in Figure 3. The results in the figure are obtained based on the open dataset Widar [23]. The data used here are collected in a classroom with a person walking in a square track and fixed communication Tx and Rx. Thus, the Doppler frequency is varying over time. We note that each estimation in the figure is obtained based on a limited number of consecutive symbols, where the sensing parameters are approximately constant. Thus, the signal model in (1) applies to each estimation. The main issue with CACC is the mirrored dynamic paths, which, as seen in Figure 3, can lead to false yet symmetric moving path detection. The CASR can mitigate the issue, particularly in single dynamic-path scenarios.

Recently, the performance bounds for Doppler sensing using the CASR method have been provided in [24] via deriving closed-form Cramer-Rao lower bound expressions. The impacts of numerous system parameters on Doppler sensing are disclosed. Waveform optimization based on the insights is also conducted, achieving substantial performance improvement.

To utilize the CSI ratio for multitarget sensing, a Taylor series-based method is proposed in [17]. A general model with multiple dynamic targets is considered in the work. The second-order complex Taylor series of the CSI ratio is derived with a closed-form expression in terms of the vector of sensing parameters to be estimated. This reveals the unique patterns embedded in the differences between CSI ratios over different snapshots, facilitating superresolution multitarget Doppler sensing. In [19], instead, independent component analysis is used to separate the multiple targets' contribution to the CFR, thus extending CASR to multitarget scenarios but entailing higher computational costs.

We remark that when more than one transmitting antennas is used, virtual antenna channels can be created at the sensing Rx side, as in conventional MIMO radar processing. Referring to the channel matrix in (1), one can see that vectorizing the

matrix can generate a new steering vector, which can be seen as the Kronecker product of the original steering vectors. Each entry of the vectorized channel vector can be seen as the CSI for a virtual channel. Nevertheless, we note that this spatial-domain processing does not change the fact that the nuisance caused by the random offsets, i.e., $\xi_{i,k}$ in (1), is still common to all entries in the CSI. This enables us to continue applying the offset elimination methods reviewed in this section to suppress the random offsets caused by clock asynchronism. However, sensing methods based on virtual channels after canceling offsets may need further investigation.

Offset Cancellation Methods: Delay-Domain Processing Techniques

Delay-domain techniques remove TO and CFO by exploiting the fact that they do not change in different signal propagation paths since they depend on the Rx hardware. Such techniques are, therefore, independent of the number of antennas at the Tx or Rx devices, and they can work in single-input, single-output systems (where cross-antenna techniques are not applicable) or systems equipped with a single phased array. To see this, we simplify the CFR model for an OFDM system given in (2) using $M = 1$ and $N = 1$. The channel gain for the kth symbol at subcarrier i is written as

$$H_{i,k} = \xi_{i,k} \sum_{l=1}^{L} b_l e^{-j2\pi i \Delta_f \tau_l} e^{j2\pi f_{D,l} k T_s}. \tag{7}$$

The aforementioned model also holds if the Tx and Rx are equipped with phased arrays of multiple antennas connected to the same RF chain. In this case, we consider the overall beamforming gain to be included in the coefficients b_l. Equation (7) suggests that a viable method to compensate for the phase offsets is to use one of the propagation paths as a reference. The phase differences concerning the reference path depend only on the propagation path delay and Doppler shift since $\xi_{i,k}$ cancels out. Hence, provided that the delay and Doppler of the reference path are known (e.g., because it is static so that the Doppler shift is absent and its delay can be estimated once using localization), estimation of the sensing parameters can be performed with low-complexity algorithms. This idea is similar to the one behind the spatial-domain (i.e., cross-antenna) processing techniques discussed in the "Offset Cancellation Methods: Spatial-Domain Processing" section, but it does not require the use of multiple antennas, leveraging multipath resolution in the delay domain instead.

The CFR contribution of the reference path, $\bar{H}_{i,k}$, is expressed as $\bar{H}_{i,k} = \xi_{i,k} b_1 e^{-j2\pi i \Delta_f \tau_1} e^{j2\pi f_{D,1} k T_s}$, where we assume by convention that the reference path has an index $l = 1$. The offset-free CFR $\hat{H}_{i,k}$ is obtained by multiplying the CFR in (7) by the complex-conjugate (to obtain phase differences) of the reference path's CFR, i.e.,

$$\hat{H}_{i,k} = H_{i,k} \bar{H}^*_{i,k} = b_1 \sum_{l=1}^{L} b_l e^{-j2\pi i \Delta_f (\tau_l - \tau_1)} e^{j2\pi (f_{D,l} - f_{D,1}) k T_s}. \tag{8}$$

In (8), the delay and Doppler parameters of path l have been replaced by the relative quantities $\tau_l - \tau_1$ and $f_{D,l} - f_{D,1}$. However, unlike in spatial-domain techniques (see the "Offset Cancellation Methods: Spatial-Domain Processing" section) here, this does not increase the subsequent parameter estimation complexity for the following two reasons. First, in both LoS and non-LoS (NLoS) conditions, relative delays $\tau_l - \tau_1$ can be easily used to track targets by exploiting the well-known bistatic radar geometry if the distance between Tx and Rx is known (see, e.g., [25]). Second, if the reference path used to compensate for CFO is static, we have $f_{D,1} = 0$, which means that the relative Doppler shifts in (8) become equal to the absolute ones. This allows for the direct estimation of the Doppler frequency, avoiding the ambiguity of relative frequency shift.

In the following, we detail SHARP, the delay-domain phase offsets compensation technique used in [18], for OFDM IEEE 802.11ac/ax systems operating on the 5-GHz Wi-Fi bands. Delay-domain processing is also used in [22], which includes a hybrid approach and will be presented in the "Hybrid Methods" section.

In SHARP, the strongest propagation path is used as the reference by reasonably assuming that it corresponds to the LoS path and remains almost unchanged over a short acquisition time. The main challenge of applying delay-domain phase offset removal in sub-7-GHz systems is their low multipath resolution due to the small transmission bandwidth (typically 40 to 160 MHz). This makes it hard to separate the multiple propagation paths by simply applying inverse Fourier transformations over the time dimension. To address the challenge, [18] proposed a custom multipath resolution technique based on the compressive sensing-based optimization problem

$$\mathbf{r}_k = \underset{\tilde{\mathbf{r}}}{\operatorname{argmin}} \left\| \mathbf{H}_k - \mathbf{T}\tilde{\mathbf{r}} \right\|_2^2 + \lambda \| \tilde{\mathbf{r}} \|_1 \tag{9}$$

where $\mathbf{H}_k = [H_{0,k}, \ldots, H_{S-1,k}]^{\mathrm{T}}$, $\mathbf{T}$ is an $(S \times L')$-dimensional dictionary matrix with element (i, l) set to $T_{i,l} = e^{-j2\pi i \tau_{l,\mathrm{tot}}/To}$, and $\tau_{l,\mathrm{tot}}$ with $l = 0, \ldots, L' - 1$ is a set of candidate combined TOs, including the propagation delay, τ_l, and the TO, $\tau_{\mathrm{o},k}$. $L' > L$ is the parameter that defines the grid of possible multipath components included in the matrix $\mathbf{T}$. The vector $\mathbf{r}_k$ (and, in turn, $\tilde{\mathbf{r}}$) is L'-dimensional and represents the subcarrier-independent terms of the offset, including the CFO and the random phase offset, i.e., element l of $\mathbf{r}_k$ is $r_{k,l} = \beta_k e^{j2\pi f_{o,k} k T_s} b_l$.

Note that in our model in (2), b_l includes a carrier phase term, $e^{-j2\pi f_c \tau_l}$, with f_c being the carrier frequency, which is instead made explicit in [18]. The position of the nonzero entries in vector $\mathbf{r}_k$, obtained by solving (9), indicate the estimated multipath components out of the L' ones. The estimate of the multipath decomposition of matrix $\mathbf{H}_k$, for each OFDM subcarrier i, is obtained by combining $\mathbf{r}_k$ and the ith row of $\mathbf{T}$, denoted by $\mathbf{T}_i$, through the Hadamard product, i.e., $\mathbf{X}_{i,k} = \mathbf{T}_i^{\mathrm{T}} \circ \mathbf{r}_k$. Finally, $\hat{H}_{i,k}$ in (8) is obtained as $\hat{H}_{i,k} = \Sigma_{l=1}^{L'} \mathbf{X}_{i,k} X^*_{i,k,0}$, where $X_{i,k,0}$ is

the first element of vector $\mathbf{X}_{i,k}$ and is associated with the strongest multipath component.

Example results on human micro-Doppler spectrogram extraction, comparing CASR and SHARP, are shown in Figure 4. The results refer to an IEEE 802.11ac testbed with a 5-GHz carrier frequency.

Offset Estimation Methods

Different from the aforementioned methods using the spatial or time domain features to cancel the random phase offsets caused by the clock asynchronism, i.e., $\xi_{i,k}$ in (2), the designs in [19], [20], and [21] seek to estimate and compensate the offset for high-performance Doppler sensing. The rationale can be seen from (4)—if only static paths are left in the denominator, the Doppler estimation would not suffer from the nonlinearity caused by the CASR anymore.

A spatial-domain linear combination is adopted in [19] and [20] to suppress the signals associated with the dynamic paths. The starting point of such designs is the transceiving relationship in the spatial domain, as embedded in the steering vectors in (2). More specifically, $\mathbf{H}_{i,k}$ therein can be seen as a linear combination of $\mathbf{a}(N,\phi_l)\mathbf{a}^{\mathrm{T}}(M,\theta_l)$, which is the outer product of two steering vectors concerning transmitting and receiving arrays. This outer product mainly conveys the spatial information of a path. Based on the matrix manipulation rule that $\mathrm{vec}(\mathbf{ABC}) = \mathbf{C}^{\mathrm{T}} \otimes \mathbf{A}\mathrm{vec}(\mathbf{B})$, where $\otimes$ denotes the Kronecker product, we can vectorize $\mathbf{H}_{i,k}$ and obtain

$$\mathrm{vec}(\mathbf{H}_{i,k}) = \underbrace{\left[\mathbf{a}(M,\theta_1)\otimes\mathbf{a}(N,\phi_1),\ldots,\mathbf{a}(M,\theta_L)\otimes\mathbf{a}(N,\phi_L)\right]}_{\mathbf{A}}\mathbf{b}_{i,k} \tag{10}$$

where $\mathbf{b}_{i,k}$ is a column vector collecting the coefficients of the L paths in (2). The aforementioned conversion is similar to conventional MIMO radar processing, where M Tx antennas and N Rx antennas can lead to MN virtual antennas. Using array signal processing theories, we see that it is theoretically feasible to identify the null space of dynamic paths. Projecting the CSI signals onto the null space can then facilitate the estimation of channel coefficients associated with the static path.

To achieve this, an optimization is performed in [19] to find the linear combination over virtual antennas that minimizes the ratio of respiration energy to the overall signal energy. The respiration energy is the signal energy in the frequency range caused by human respiratory movement, which can be determined based on system configurations, such as carrier frequency and the transceiver's geometric relationship. In [20], the MUSIC algorithm estimates the AoAs of static and dynamic paths. It is shown in the work that, in the presence of a strong LoS path, the Bartlett beamformer would form a peak at the LoS path. This feature is then used to differentiate the LoS path's AoA from those of dynamic paths. The null space of the dynamic paths in the spatial domain is then constructed to extract the LoS path, which facilitates the estimation of the composite random phase caused by the asynchronism, $\xi_{i,k}$. Similarly, the null space method extracts each dynamic path by suppressing others, enabling the estimation of their Doppler frequencies.

If a strong LoS path exists and only the Doppler information is of interest, estimating and compensating for the asynchronism offsets can be quite effective by fully taking advantage of the LoS path. This is demonstrated in [21]. By treating the first path in (1) as the strong LoS path, then $b_1 e^{-j2\pi i(\tau_1+\tau_{o,k})\Delta_f}$ can be seen as a single-tone signal indexed by the subcarrier index i. Estimating the frequency of this signal gives us an estimate of the composite delay with the LoS path delay plus TO. We refer interested readers to [21] and [26] for the details on the estimation method. It is based on discrete Fourier transform (DFT) interpolation, a popular low-complexity frequency estimation method with off-grid accuracy. With the composite delay of the LoS path, i.e., $\tau_1 + \tau_{o,k}$, estimated, signals can be coherently accumulated over the LoS path, and the phase of the high signal-to-noise ratio (SNR) accumulated signal can be used as the estimation of all other random phase offsets. This method applies to any antenna and symbol as seen in (1).

Hybrid Methods

In [22], a hybrid method, named *JUMP*, which combines TO estimation and suppression with CFO estimation, was proposed for a millimeter-wave (mmWave) system based on IEEE 802.11ay. mmWave systems offer a wide transmission

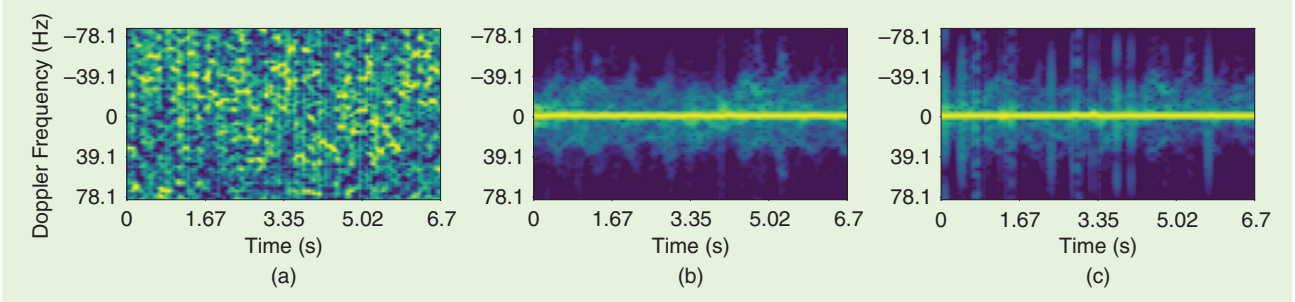

FIGURE 4. An example human micro-Doppler with a 5-GHz carrier frequency (IEEE 802.11ac). In (a), the spectrum is affected by CFO. In (b) and (c), the phase offset was removed using (b) CASR [16] and (c) SHARP [18]. Powers are normalized between 0 (blue) and 1 (yellow). (a) With CFO. (b) CASR. (c) SHARP.

bandwidth that, in turn, leads to higher multipath resolution than in sub-7-GHz ones. This makes mmWave systems the ideal application scenario for delay-domain techniques (see the "Offset Cancellation Methods: Delay-Domain Processing Techniques" section) since multipath separation is easily achieved by detecting the peaks of the CIR. The latter is obtained as part of the communication protocol to perform channel equalization in single carrier (SC) systems (like IEEE 802.11ay), while it can be obtained via inverse DFT in OFDM systems. Recalling that $\xi_{i,k} = \beta_k e^{-j2\pi i \Delta_f \tau_{o,k}} e^{j2\pi f_{o,k} k T_s}$, the CIR model corresponding to the CFR in (7) is

$$h_{n,k} = \beta_k \sum_{l=1}^{L} b_l e^{j2\pi (f_{D,l} + f_{o,k}) k T_s} \delta_{n-\tau_l-\tau_{o,k}} \tag{11}$$

where n is the index of delay-domain samples spaced by $1/B$ and δ_n is the Kronecker delta. Note that, in (11), using Kronecker delta functions is an approximation of the real CIR that neglects the impact of the nonideal autocorrelation of pilot sequences and sampling points in SC systems or the finite bandwidth in OFDM ones. We neglect such nonidealities, as done in [22] to maintain the same notation.

From (11), one can see that the effect of TO is a shift of the CIR by $\tau_{o,k}$, while the CFO affects the phase of the CIR. Ref. [22] presents a hybrid algorithm that first estimates and compensates for the TO and then cancels out the CFO using a delay-domain approach. The two processing steps are detailed next.

1) *TO estimation and compensation:* The multiple propagation paths appear as peaks in the magnitude of the estimated CIR at the Rx, which can be detected, e.g., by defining a suitable threshold or by more advanced adaptive methods [22]. Then, the first detected path, having the lowest delay, is the LoS path to be used as a reference. The TO appears as a common shift of all propagation paths, so it can be removed by estimating the LoS path peak location, equal to $\tau_1 + \tau_{o,k}$, and applying an opposite shift to the CIR by convolving it with $\delta_{n+\tau_1+\tau_{o,k}}$.
2) *CFO cancellation:* This second step is based on the delay-domain approach. The phase of a static reference path, i.e., having $f_{D,1} = 0$, is extracted. Such a phase contains the nuisance due to $f_{o,k}$ and $\angle\beta_k$, so the CFO and random phase offset are removed from the CIR by computing $\hat{h}_{n,k} = \tilde{h}_{n,k} e^{-j\angle\tilde{h}_{1,k}}$, where $\tilde{h}_{1,k}$ is the TO-free CIR resulting from point 1).

The resulting CIR allows estimating relative delays and Doppler frequencies with low-complexity algorithms. As an example, in [22], this is done by applying peak detection to the CIR magnitude to obtain $\tau_l - \tau_1$ with $l = 1, \ldots, L$ from the locations of the peaks. Then, $f_{D,l}$ are estimated by performing a DFT over a window of K CIR samples. The Doppler frequencies correspond to the peaks in the Doppler spectrum, computed as the squared magnitude of the DFT.

Example results showing the effect of CFO compensation on a human micro-Doppler spectrogram are shown in Figure 5. The experimental data were obtained using a field-programmable gate array-based IEEE 802.11ay system with a 60-GHz carrier frequency.

The previous offsets compensation technique is then extended to the case where the LoS path is not always available, e.g., because it is temporarily blocked by an obstacle. The approach relies on the assumption that the channel contains multipath reflections on static objects, which are slowly time varying compared to the packet transmission rate, which is a common assumption for radar and ISAC. The technique leverages the similarity of the CIR magnitude profiles across subsequent packets and performs the following steps:

1) *Estimation of the relative TO between subsequent CIR estimates, defined as* $\tau_o^r \triangleq \tau_{o,k} - \tau_{o,k-1}$*:* This can be done, e.g., by locating the correlation peak for different candidate shift values between the CIR amplitude profiles $|h_{n,k}|$ and $|h_{n,k-1}|$.
2) *Compensation of the relative TO by shifting* $h_{n,k}$ *by* τ_o^r*:* When applied sequentially to subsequent CIR estimates for $k = 0, \ldots, K-1$, this step incrementally removes the TO.

Thanks to step 1, any static path can be used as a reference since the CIR samples across time share the same timing reference. Selecting a reference path different from the LoS may be challenging when CFO is present since the distinction between static paths and dynamic ones cannot be made based on the corrupted Doppler shift. In [22], this is solved by applying a tracking algorithm to the multipath components of the CIR to estimate the location of the scatterer in the 2D Cartesian plane after TO has been compensated for. Static paths are identified as the ones whose position does not change significantly across time, and the reference path is selected as the static path with the highest amplitude.

To initialize the algorithm, [22] assumes that the sensing operation starts in a LoS condition, where the TO can be removed, or that the LoS becomes available at least once during

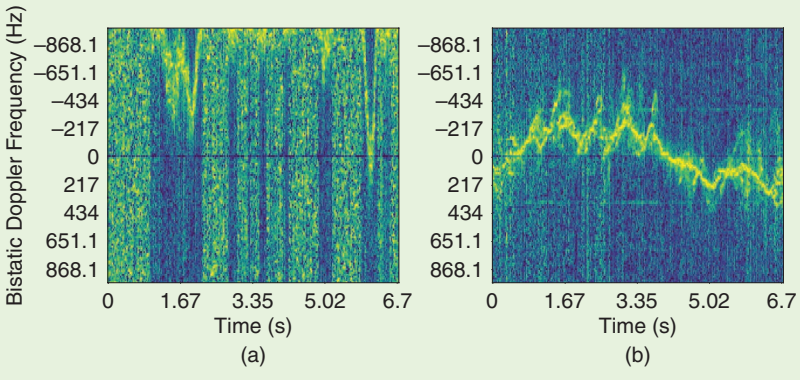

FIGURE 5. An example human micro-Doppler with 60-GHz carrier frequency (IEEE 802.11ay). In (a), the micro-Doppler spectrum is affected by CFO. In (b), we apply JUMP [22] to remove it. Powers are normalized between 0 (blue) and 1 (yellow).

the system operation. Under this assumption, the compensation of the relative TOs between subsequent packets by steps 1 and 2 allows for maintaining the LoS-based timing reference even when transitioning to NLoS conditions for intermittent time intervals. Note that the previous technique depends on the fact that transitions between LoS and NLoS conditions are slow compared to variations of the CIR magnitude profile. This makes it appealing for indoor scenarios, in which it is likely to have multiple static propagation paths (e.g., from reflections on the walls). Conversely, due to its sensitivity to abrupt changes in the multipath profile, this technique may not be suitable for highly dynamic outdoor scenarios.

Comparisons and Remarks

Table 1 compares all methods reviewed previously regarding their requirements and features, where OTA stands for "over the air." The three types are stated at the beginning of the "Single-Node Bistatic Sensing Techniques" section, where the first type is further divided into two subtypes, with the spatial-domain methods, under the type I(S) in the table reviewed in the "Offset Cancellation Methods: Spatial-Domain Processing" section, and the delay-domain method, under I(D), reviewed in the "Offset Cancellation Methods: Delay-Domain Processing Techniques" section. In Table 1, the three domains are mainly referred to as where the offsets are addressed. As mentioned earlier, most works are predominantly performed in the spatial domain. However, some recent works incorporate other domains to relieve the reliance on multiple antennas and explore the degrees of freedom available.

Moreover, not all methods can sense multiple targets concurrently moving in the environment. Specifically, CACC and delay-domain techniques support multiple targets, subject to having enough bandwidth and/or AoA resolution to resolve the corresponding multipath components. Conversely, CASR is mainly applicable to single-target scenarios and requires special processing to separate the multiple contributions, as shown in [17] and [19].

As a sensing-related application, positioning or localization in 5G and beyond networks is emerging as a hot research topic [28], [29]. In such applications, TO is of particular interest as the time of arrival is typically a key sensing parameter used in localization algorithms. In [28], a time difference of arrival is proposed to counteract TOs. In [29], a novel maximum likelihood estimator is developed to estimate TO and other sensing parameters, such as multipath angles. While the TO can be estimated using these approaches, they do not sufficiently treat the frequency offset and random phase. In bistatic sensing, the methods reviewed in the "Offset Cancellation Methods: Delay-Domain Processing Techniques," "Offset Estimation Methods," and "Hybrid Methods" sections may be further applied on top of these approaches [28], [29]; alternatively, it can also be interesting to extend the methods [28], [29] with the other two types of offsets taken into account.

We remark that the ideas behind the methods reviewed in this section are promising to be applicable in the 6G context for addressing clock offsets, although quite a number of them are developed in the Wi-Fi sensing background. This is because, regardless of network differences, the MIMO-OFDM waveform is used by both cellular and Wi-Fi networks, and all the reviewed methods can apply to a general MIMO-OFDM setup. However, it is noteworthy that, when applying these methods to the 6G network, adaptions/changes may be necessary due to the potentially different features of 6G networks compared with Wi-Fi, as highlighted next.

- The 6G base station may be equipped with the so-called massive MIMO arrays, which can be efficiently applied to achieve great spatial resolution and separate multiple objects to be sensed. mmWave systems will likely be hybrid arrays with analog beamforming before their digital counterparts. This means that the cross-antenna techniques [12], [13], [14], [15], [16], [17] will need to be extended to deal with cross-beam signals. Moreover, analog beamforming may be designed to facilitate better solutions to addressing clock offsets.
- 6G is expected to have a much larger frequency bandwidth than Wi-Fi, leading to more degrees of freedom in the time-frequency-domain resources. These can further improve some of the methods reviewed in this section. For

Table 1. A comparison of different bistatic sensing techniques.

Type	Methods	Strong LoS	Multiple Targets	Single Antenna	Processing Domain	Doppler-AoA Only	OTA
I(S)	Indotrack [12]	✓	✗	✗	S	✓	✓
	WiDFS [13]	✓	✗	✗	S	✓	✓
	CACC [14]	✓	✓	✗	S	✓	✗
	FarSense [15]	✗	✗	✗	S	✓	✓
	CASR [16]	✗	✗	✗	S	✓	Widar
	CASR [17]	✗	✓	✗	S	✓	WiDFS
I(D)	SHARP [18]	✗	✗	✓	D	✗	✓ [27]
II	multiSense [19]	✗	✓	✗	S, F	✓	✓
	[20]	✓	✓	✗	S	✓	✓
	[21]	✓	✓	✓	F	✓	Widar
III	JUMP [22]	✗	✓	✓	D	✗	✓

S: spatial; D: delay; F: frequency; OTA: over the air.

example, the large bandwidth can be enjoyed by SHARP [18] to facilitate much higher resolution in the range domain, hence addressing clock offset issues more effectively. As another example, the waveform design in the time-frequency domain can be resorted to, as performed in [24], for better offset estimation performance.

- 6G networks may be deployed both indoors and outdoors. For indoor applications, the channels will be similar to Wi-Fi channels, and techniques validated on a Wi-Fi platform can be expected to work effectively on 6G networks. The 6G outdoor channels can be substantially different from Wi-Fi ones. This makes channel-dependent methods, such as [19] in indoor Wi-Fi scenarios, not directly applicable to 6G. However, the idea may be borrowed. For example, instead of using the respiratory movement for estimating the optimal combination over antennas (see the "Offset Estimation Methods" section for more details), the varying channels caused by a car's movement in a rural area can be relied on in 6G outdoor sensing to achieve similar goals.

Future Research Directions and Open Problems

We have seen promising advances in addressing the clock asynchronism in bistatic ISAC. However, admittedly, many open problems still need more attention from the academia and industry communities.

The previous discussion on the techniques enables us to formulate a comprehensive framework, laying the groundwork for future research at an elevated level. This framework, depicted in Figure 6, is 2D. One dimension encompasses signal processing methods, including reference signal construction, offset estimation, and offset cancellation via the cross-correlation and signal ratio. The second dimension pertains to the domains where signal processing is primarily applied, with the typical space and delay domains. These methods have the flexibility to be implemented individually or in combination across one or more domains. While existing works, as explored in the "Single-Node Bistatic Sensing Techniques" section, have substantiated feasibility and demonstrated potential, a thorough examination of the advantages and disadvantages of these methods and their application domains reveals opportunities for further refinement and exploration. A summary of the examination is as follows:

- Constructing a reference signal can simplify the subsequent sensing parameter estimation, but it will inevitably introduce errors.
- Offset estimation enables flexible signal processing. However, it also faces estimation errors, which could be larger than those in reference signal construction.
- Offset cancellation exploits signal structures and removes offsets without introducing errors. However, it typically leads to more parameters to be estimated (signal cross-correlation) or a nonlinear problem (signal ratio).
- Spatial-domain processing well retains independence of paths in the delay and Doppler domains, but multiple receiving chains are required, which may not be cost-effective, particularly for mmWave systems.
- Delay-domain processing requires only a single receive antenna, but obtaining CIR is sometimes challenging in OFDM systems when measurements are available only at a part of the subcarriers. In addition, each CIR may be the superposition of multiple paths when delays are off grid.

Therefore, a proper combination can be designed by jointly considering the respective advantages and disadvantages of these methods and domains, together with additional signal and system factors, as shown in Figure 6. By delineating the 2D landscape of signal processing methods and their application domains, novel combinations and innovations may be achieved. Within the framework, some more specific research problems are elaborated next.

Construction of a Reference Path

The efficient and reliable construction of a reference path is an interesting open research challenge in delay-domain processing techniques to enable phase offset compensation. Ref. [22] proposed to apply tracking algorithms to maintain an estimate of several candidate reference paths, including first-order reflections on static objects. However, the sensing accuracy depends on the signal quality received from the reference path and degrades with low SNR.

Sensing of Multiple Targets

To the best of our knowledge, only two works ([19] and [22]) have experimentally validated phase offset removal techniques (hybrid, delay domain, and CASR, respectively) on data collected with multiple sensing targets concurrently moving in the environment. Cross-antenna techniques do not work out of the box in such cases, and techniques to separate the contributions of the different subjects are required, as detailed in the "Cross-Antenna Signal Ratio" section. Reference path-based techniques are not affected by multiple targets.

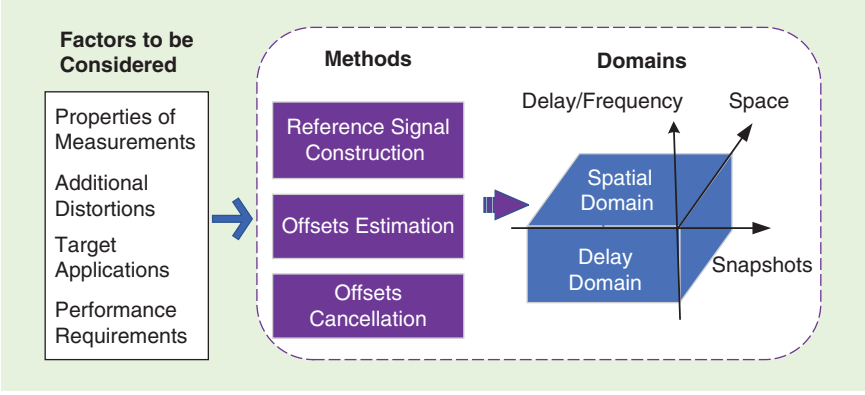

FIGURE 6. A generalized framework for solutions to clock asynchronism in bistatic sensing.

However, obtaining a reliable reference path when multiple targets are moving, possibly causing occlusion to the LoS, is extremely challenging and deserves further attention from the research community.

Mobility of the Nodes

Performing ISAC with mobile nodes is a challenging problem in the presence of phase offsets. Notably, the assumption that the Tx and Rx are static is critical to all three phase offset removal techniques. To our knowledge, only [30] has presented a preliminary dynamic CFR model for Wi-Fi sensing, but it does not deal with phase offsets. Possible approaches to tackle this problem may come from the passive radar literature, where radars mounted on moving platforms are well studied, e.g., [31].

Coherently Combine Multiple Rxs

To fully exploit the potential of pervasive ISAC, algorithms that combine the information from multiple phase-synchronized Rxs need to be developed. This would boost the system's sensing resolution, overcoming the limitation imposed by the bandwidth and enabling wavelength-level sensing accuracy. To enable this, algorithms that effectively remove the different phase offsets between each Tx-Rx must be investigated to allow the coherent fusion of the data obtained at each Rx. A preliminary study on this subject can be found in [32].

Joint Spatial-Delay-Frequency-Domain Processing

From Table 1, we see that existing designs generally utilize one or two but not all three domains (spatial, delay, and frequency) for addressing the clock asynchronism. This contributes to the restrictions of existing methods, e.g., having a strong LoS, large bandwidth, or a single dynamic path, that are often associated with which domain we use for phase offset compensation. For instance, many spatial and frequency-domain methods require strong LoS, which is unnecessary for the delay-domain methods. However, the performance of the delay-domain method may be subject to the bandwidth available, while the other domains are not. Jointly using the three domains can allow us to exploit and combine the advantages of different approaches, promising to remove the restrictions suffered by most existing works.

Open Dataset for Bistatic Sensing Research and Development

While most works reviewed in the "Single-Node Bistatic Sensing Techniques" section perform OTA experiments to validate their methods, custom configurations and hardware platforms are often heterogeneous and do not follow unified standards. For this purpose, only a few publicly available open datasets, such as those mentioned in Table 1, are available. Moreover, most existing works and experiments are based on Wi-Fi protocols/platforms. Other wireless systems, such as mobile networks, have been validated in a few works, such as [9]. Therefore, a critical aspect for advancing bistatic sensing further is the availability of a comprehensive open dataset based on different communications protocols in various yet typical sensing scenarios that can be used to assess and compare the performance of the proposed approaches.

Concluding Remarks

In this survey, we have provided a first review of the clock asynchronism issue in bistatic sensing against the highly popular ISAC background. We started by establishing the MIMO-OFDM signal model, which is widely used in modern communications systems. We then modeled and explained the impact of random offsets caused by the clock asynchronism issue on bistatic sensing. Moreover, we reviewed three major solutions to the issue as differentiated by whether the offsets are cancelled, estimated, and suppressed or are treated in a hybrid way. The basic signal processing principles of the reviewed techniques are highlighted, and some interesting results are demonstrated. After comparing all reviewed methods, we drew insights into potential research directions and open problems. We hope that our first survey article on this topic can foster more research activities on maturing bistatic sensing in ISAC.

Acknowledgment

This work was partially supported by the European Union under the Italian National Recovery and Resilience Plan (NRRP) of NextGenerationEU, partnership on "Telecommunications of the Future" (PE0000001 – program "RESTART"). This work is supported in part by the National Science Foundation under Grants CCF-2218845, ECCS-2229472, and ECCS-2329013, by the Office of Naval Research under Grant N00014-23-1-2221, and by the Air Force Office of Scientific Research under Grant FA9550-23-1-0261. This work is partially supported by the Australian Research Council under Grant DP210101411.

Authors

Kai Wu (kai.wu@uts.edu.au) is a lecturer with the Global Big Data Technologies Centre, School of Electrical and Data Engineering, University of Technology Sydney, Sydney NSW 2007, Australia. He is a Member of IEEE.

Jacopo Pegoraro (pegoraroja@dei.unipd.it) is a postdoctoral researcher and lecturer in the Department of Information Engineering, University of Padova, 35122 Padova, Italy. He is a Member of IEEE.

Francesca Meneghello (francesca.meneghello.1@unipd.it) is an assistant professor with the Department of Information Engineering, University of Padova, 35122 Padova, Italy. She is a Member of IEEE.

J. Andrew Zhang (andrew.zhang@uts.edu.au) is a professor in the School of Electrical and Data Engineering, University of Technology Sydney, Sydney NSW 2007, Australia. He is a Senior Member of IEEE.

Jesus O. Lacruz (jesusomar.lacruz@imdea.org) has been a research engineer at IMDEA Networks, 28918 Madrid, Spain, since 2017.

Joerg Widmer (Joerg.Widmer@imdea.org) is a research professor and research director at IMDEA Networks, 28918 Madrid, Spain. He is a Fellow of IEEE.

Francesco Restuccia (f.restuccia@northeastern.edu) is an assistant professor of electrical and computer engineering at Northeastern University, Boston, MA 02115 USA. He is a Senior Member of IEEE.

Michele Rossi (michele.rossi@unipd.it) is a full professor at the Department of Information Engineering and the Department of Mathematics of the University of Padova, 35122 Padova, Italy. He is a Senior Member of IEEE.

Xiaojing Huang (xiaojing.huang@uts.edu.au) is currently a professor of information and communications technology with the School of Electrical and Data Engineering and the program leader for mobile sensing and communications with the Global Big Data Technologies Center, University of Technology Sydney, Sydney NSW 2007, Australia. He is a Senior Member of IEEE.

Daqing Zhang (daqing.zhang@telecom-sudparis.eu) is a professor at Peking University, Beijing 100871, China, and IP Paris, 91120 Palaiseau, France. He is a Fellow of IEEE and a member of the Academy of Europe.

Giuseppe Caire (caire@tu-berlin.de) is an Alexander von Humboldt Professor with the Faculty of Electrical Engineering and Computer Science at the Technical University of Berlin, 10587 Berlin, Germany. They are a Fellow of IEEE.

Y. Jay Guo (jay.guo@uts.edu.au) is a Distinguished Professor and the funding director of the Global Big Data Technologies Centre at the University of Technology Sydney, Sydney NSW 2007, Australia. He is the founding technical director of the New South Wales Connectivity Innovation Network. He is a Fellow of IEEE.

References

[1] A. Graff, Y. Chen, N. González-Prelcic, and T. Shimizu, "Deep learning-based link configuration for radar-aided multiuser mmWave vehicle-to-infrastructure communication," *IEEE Trans. Veh. Technol.*, vol. 72, no. 6, pp. 7454–7468, Jun. 2023, doi: 10.1109/TVT.2023.3239227.

[2] K. V. Mishra, M. Bhavani Shankar, V. Koivunen, B. Ottersten, and S. A. Vorobyov, "Toward millimeter-wave joint radar communications: A signal processing perspective," *IEEE Signal Process. Mag.*, vol. 36, no. 5, pp. 100–114, Sep. 2019, doi: 10.1109/MSP.2019.2913173.

[3] J. A. Zhang et al., "Enabling joint communication and radar sensing in mobile networks–a survey," *IEEE Commun. Surv. Tuts.*, vol. 24, no. 1, pp. 306–345, Firstquarter 2022, doi: 10.1109/COMST.2021.3122519.

[4] J. A. Zhang, A. Cantoni, X. Huang, Y. J. Guo, and R. W. Heath, "Framework for an innovative perceptive mobile network using joint communication and sensing," in *Proc. IEEE 85th Veh. Technol. Conf. Spring*, Sydney, NSW, Australia, 2017, pp. 1–5.

[5] A. Kumar. "ITU approves 6G vision framework." ET Telecom. Accessed: Aug. 27, 2023. [Online]. Available: https://telecom.economictimes.indiatimes.com/news/policy/itu-approves-6g-vision-framework/101184232

[6] J. A. Zhang, K. Wu, X. Huang, Y. J. Guo, D. Zhang, and R. W. Heath, "Integration of radar sensing into communications with asynchronous transceivers," *IEEE Commun. Mag.*, vol. 60, no. 11, pp. 106–112, Nov. 2022, doi: 10.1109/MCOM.003.2200096.

[7] J. A. Zhang et al., "An overview of signal processing techniques for joint communication and radar sensing," *IEEE J. Sel. Topics Signal Process.*, vol. 15, no. 6, pp. 1295–1315, Nov. 2021, doi: 10.1109/JSTSP.2021.3113120.

[8] V. C. Chen, F. Li, S.-S. Ho, and H. Wechsler, "Micro-Doppler effect in radar: Phenomenon, model, and simulation study," *IEEE Trans. Aerosp. Electron. Syst.*, vol. 42, no. 1, pp. 2–21, Jan. 2006, doi: 10.1109/TAES.2006.1603402.

[9] Y. Feng, Y. Xie, D. Ganesan, and J. Xiong, "LTE-based pervasive sensing across indoor and outdoor," in *Proc. 19th ACM Conf. Embedded Netw. Sens. Syst. Ser. SenSys*, New York, NY, USA: Association for Computing Machinery, 2021, pp. 138–151, doi: 10.1145/3485730.3485943.

[10] W.-C. Liu, T.-C. Wei, Y.-S. Huang, C.-D. Chan, and S.-J. Jou, "All-digital synchronization for SC/OFDM mode of IEEE 802.15. 3c and IEEE 802.11ad," *IEEE Trans. Circuits Syst.*, vol. 62, no. 2, pp. 545–553, Oct. 2014, doi: 10.1109/TCSI.2014.2361035.

[11] T. M. Schmidl and D. C. Cox, "Low-overhead, low-complexity burst synchronization for OFDM," in *Proc. ICC/SUPERCOMM-Int. Conf. Commun.*, Dallas, TX, USA, 1996, vol. 3, pp. 1301–1306.

[12] X. Li et al., "IndoTrack: Device-free indoor human tracking with commodity Wi-Fi," in *Proc. ACM Interact. Mob. Wearable Ubiquitous Technol.*, Sep. 2017, pp. 1–22, doi: 10.1145/3130940.

[13] Z. Wang, J. A. Zhang, M. Xu, and Y. J. Guo, "Single-target real-time passive Wifi tracking," *IEEE Trans. Mobile Comput.*, vol. 22, no. 6, pp. 3724–3742, Jun. 2023, doi: 10.1109/TMC.2022.3141115.

[14] Z. Ni, J. A. Zhang, X. Huang, K. Yang, and J. Yuan, "Uplink sensing in perceptive mobile networks with asynchronous transceivers," *IEEE Trans. Signal Process.*, vol. 69, pp. 1287–1300, 2021, doi: 10.1109/TSP.2021.3057499.

[15] Y. Zeng, D. Wu, J. Xiong, E. Yi, R. Gao, and D. Zhang, "FarSense: Pushing the range limit of Wifi-based respiration sensing with CSI ratio of two antennas," in *Proc. ACM Interactive, Mob. Wearable Ubiquitous Technol.*, vol. 3, no. 3, pp. 1–26. Sep. 2019, doi: 10.1145/3351279.

[16] X. Li, J. A. Zhang, K. Wu, Y. Cui, and X. Jing, "CSI-ratio-based Doppler frequency estimation in integrated sensing and communications," *IEEE Sensors J.*, vol. 22, no. 21, pp. 20,886–20,895, Nov. 2022, doi: 10.1109/JSEN.2022.3208272.

[17] Z. Ni, J. A. Zhang, K. Wu, and R. P. Liu, "Uplink sensing using CSI ratio in perceptive mobile networks," *IEEE Trans. Signal Process.*, vol. 71, pp. 2699–2712, 2023, doi: 10.1109/TSP.2023.3294626.

[18] F. Meneghello, D. Garlisi, N. D. Fabbro, I. Tinnirello, and M. Rossi, "SHARP: Environment and person independent activity recognition with commodity IEEE 802.11 access points," *IEEE Trans. Mobile Comput.*, vol. 22, no. 10, pp. 6160–6175, Oct. 2022, doi: 10.1109/TMC.2022.3185681.

[19] Y. Zeng, D. Wu, J. Xiong, J. Liu, Z. Liu, and D. Zhang, "MultiSense: Enabling multi-person respiration sensing with commodity Wifi," in *Proc. ACM Interact, Mob. Wearable Ubiquitous Technol.*, Sep. 2020, pp. 1–29, doi: 10.1145/3411816.

[20] J. Zhao, Z. Lu, J. A. Zhang, S. Dong, and S. Zhou, "Multiple-target Doppler frequency estimation in ISAC with clock asynchronism," *IEEE Trans. Veh. Technol.*, vol. 73, no. 1, pp. 1–6, Jan. 2023, doi: 10.1109/TVT.2023.3301589.

[21] K. Wu, J. A. Zhang, X. Huang, and Y. J. Guo, "A low-complexity CSI-based Wifi sensing scheme for LoS-dominant scenarios," in *Proc. IEEE Int. Conf. Commun.*, 2023, pp. 2747–2752, doi: 10.1109/ICC45041.2023.10279247.

[22] J. Pegoraro et al., "JUMP: Joint communication and sensing with Unsynchronized transceivers Made Practical," *IEEE Trans. Wireless Commun.*, 2024, doi: 10.1109/TWC.2024.3365853.

[23] K. Qian, C. Wu, Y. Zhang, G. Zhang, Z. Yang, and Y. Liu, "Widar2.0: Passive human tracking with a single Wi-Fi link," in *Proc. 16th Annu. Int. Conf. Mobile Syst. Appl. Serv. Ser. MobiSys*, New York, NY, USA: Association for Computing Machinery, 2018, pp. 350–361.

[24] Y. Hu, K. Wu, J. A. Zhang, W. Deng, and Y. J. Guo, "Performance bounds and optimization for CSI-ratio based bi-static Doppler sensing in ISAC systems," 2024, *arXiv:2401.09064*.

[25] P. Samczyński et al., "5G network-based passive radar," *IEEE Trans. Geosci. Remote Sens.*, vol. 60, pp. 1–9, 2021, doi: 10.1109/TGRS.2021.3137904.

[26] K. Wu, J. A. Zhang, X. Huang, and Y. J. Guo, "Accurate frequency estimation with fewer DFT interpolations based on Padé approximation," *IEEE Trans. Veh. Technol.*, vol. 70, no. 7, pp. 7267–7271, Jul. 2021, doi: 10.1109/TVT.2021.3087869.

[27] F. Meneghello, N. D. Fabbro, D. Garlisi, I. Tinnirello, and M. Rossi, "A CSI dataset for wireless human sensing on 80 MHz Wi-Fi channels," *IEEE Commun. Mag.*, vol. 61, no. 9, pp. 146–152, Jun. 2023, doi: 10.1109/MCOM.005.2200720.

[28] J. Palacios, N. González-Prelcic, and C. Rusu, "Low complexity joint position and channel estimation at millimeter wave based on multidimensional orthogonal matching pursuit," in *Proc. 30th Eur. Signal Process. Conf. (EUSIPCO)*, Piscataway, NJ, USA: IEEE Press, 2022, pp. 1002–1006, doi: 10.23919/EUSIPCO55093.2022.9909920.

[29] M. A. Nazari, G. Seco-Granados, P. Johannisson, and H. Wymeersch, "Mmwave 6D radio localization with a snapshot observation from a single BS," *IEEE Trans. Veh. Technol.*, vol. 72, no. 7, pp. 8914–8928, Jul. 2023, doi: 10.1109/TVT.2023.3246303.

[30] J. Liu et al., "Towards a dynamic Fresnel zone model to Wifi-based human activity recognition," in *Proc. ACM Interactive, Mobile, Wearable Ubiquitous Technol.*, 2023, pp. 1–24, doi: 10.1145/3596270.

[31] P. Wojaczek, F. Colone, D. Cristallini, and P. Lombardo, "Reciprocal-filter-based STAP for passive radar on moving platforms," *IEEE Trans. Aerosp. Electron. Syst.*, vol. 55, no. 2, pp. 967–988, Apr. 2019, doi: 10.1109/TAES.2018.2867688.

[32] D. Tagliaferri et al., "Cooperative coherent multistatic imaging and phase synchronization in networked sensing," 2023, *arXiv:2311.07212*.